Brazilian Journal of Physics, vol. 23, no. 1, March, 1993

Modulation Spectroscopy in Semiconductor Heterostructures

Fernando Cerdeira
Instituto de Física, Universidade Estadual de Campinas
Campinas, 13081-970, SP, Brasil

Received November 9, 1992

Several techniques have been used to study the electronic states of semiconductors microstructures such as superlattices, quantum wells, planar doping structures and modulation doped heterostructures. In the present work we review some of the recent work performed in our laboratories using photo and electromodulated reflectivity and transmission on some of these microstructures. These techniques produce sharp derivative spectra taken at either room or liquid nitrogen temperatures. On the other hand, the spectra are usually rich in features, the interpretation of which is not straightforward. Thus, the ease with which experimental data is obtained is sometimes offset by the complexity of the interpretation of the spectra. This richness and complexity is illustrated with work performed in GaAs samples with two-dimensional electron gases and strained-layer superlattices and quantum wells of InGaAs/GaAs and Si/Ge.

I. Introduction

Modulation spectroscopy measures the changes in optical reflectivity or transmission when a periodic perturbation is applied to the system under study. This perturbation might be applied to the incident light beam, as in wavelength modulation, or directly to the sample (stress, temperature changes or external electric fields), thus modulating the optical properties of the material. In all cases the changes introduced are small, so that the resulting spectrum is usually related to some derivative of the un modulated spectrum. This derivative nature suppresses uninteresting backgrounds and produces sharp structures localized at the photon energy region where singular points occur in the joint density of states. The advantage of this is that these singular points, which are well localized in energy, can usually be analysed by locally-valid parabolic band models. This point is well illustrated in Fig. 1, where the reflectivity of GaAs and its wavelength and electric-field modulated relatives are portrayed. Bumps and shoulders in R, originating in van Hove singularities of the joint density of states, are highlighted in the first (wavelength modulated reflectivity) and third (low-field electroreflectance) derivative spectra (Fig.1(b) and 1(c)). It might be argued that the same result could have been obtained by recording the reflectivity and then successively differentiating this spectrum numerically. This procedure is not generally useful because repeated differentiations greatly enhance the noise present in the original spectrum. Also, by directly measuring the derivative spectrum, a variety of systematic errors, ranging from light-source fluctuations through long term drift in the electronics, is avoided.

Because of the advantages enumerated above, modulation spectroscopy had a decisive influence in understanding the band structures of bulk semiconductors. Most of the work in this area was performed in the sixties and early seventies and has been extensively reviewed by several authors. Representative examples of these reviews are listed in refs.[1-5]. With the advent of semiconductor microstructures, grown by techniques such as molecular beam epitaxy (MBE), metal-organic vapor deposition (MOCVD) and chemical beam epitaxy (CBE), a whole new realm of manmade materials has emerged, the electronic structure of which must be studied. As a consequence of this there has been a revival of interest in traditional as well as in modulated optical spectroscopy. The latter type of measurements has been very useful in studying some of these microstructures, as the recent reviews of F. H. Pollak show[6,7]. Of particular importance have been the techniques of photo and electromodulated transmission and reflectivity, which produce third-derivative lineshapes under well chosen experimental conditions[4,5]. In what follows, after a brief discussion of the experimental techniques and lineshapes, we shall review recent work performed in our laboratories with these techniques on a variety of semiconductor microstructures[8-14].

II. Experimental Techniques

The experimental set-up used in photo or electromodulated spectroscopy is shown, schematically, in Fig.

2. Modulation of built-in fields in the semiconductor microstructure can be accomplished by illuminating the sample with a secondary (pump) beam, with photon energy above the fundamental gap, chopped typically at a frequency 10 Hz $\leq$ R, $\leq 10^3$ Hz. The exact mechanism by which the injected electron-hole pairs modulate the built-in fields is very much under discussion and is sample-dependent. In most cases, however, it depends on the photo-voltaic effect, that consists in a reduction of the electric field at some interface (substrate-buffer layer, capping layer-air, etc.), in much the same way as in bulk semiconductors[15,16]. These fields also can be modulated by depositing a semi-transparent metallic film, which creates a Schottky barrier at the sample surface[5]; this barrier can be biased by an externally applied dc voltage and modulated by an ac one. Phase-sensitive detection allows the measurement of variations in the transmission or reflectivity of the sample as small as a few parts in 10^5 or 10^6. The experimental arrangement of Fig. 2 is self-explanatory and has been described in detail by other authors[1,5,6]. Such a set-up is readily mounted with simple inexpensive equipment available in most laboratories where optical measurements are performed.

The quantity directly measured is the fractional variation in the reflectivity (R) or transmissivity (T) of the material, i.e., $\Delta R/R$ or $\Delta T/T$. Theoretical calculations usually yield the dielectric response function ($\epsilon = \epsilon_1 + i\epsilon_2$). Variations in this response function are related to the experimentally obtained spectra by:

$$\frac{\Delta R}{R} = \alpha\Delta\epsilon_1 + \beta\Delta\epsilon_2 = Re[(\alpha - i\beta)\Delta\epsilon] = Re[Ce^{i\theta}\Delta\epsilon], \quad (1)$$

where α and β are the Seraphin Coefficients[3]. Similar expressions can be obtained for $\Delta T/T$.

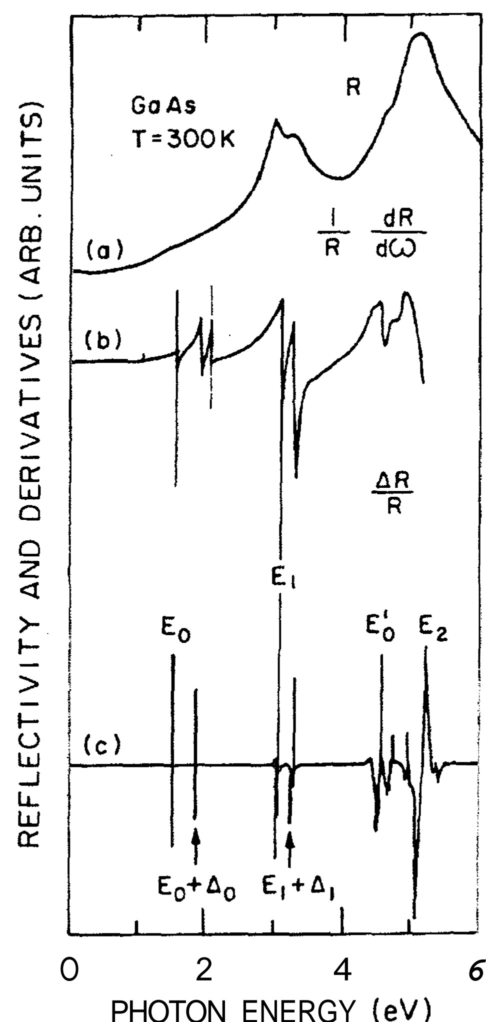

Figure 1: A comparison of three types of optical spectra for bulk GaAs: (a) reflectance, (b) energy-derivative modulation reflectivity and (c) low-field electroreflectance. From ref. [5].

III. Some Considerations on Lineshapes

III.1 General Considerations (Bulk Semiconductors)

The simplicity and relative ease with which the experiment is performed sometimes contrasts with the complexities inherent to the detailed interpretation of the resulting lineshapes. As with all modulation techniques, the perturbation introduces small changes in the complex dielectric constant of the material, ϵ. When periodicity is retained by the perturbation Hamiltonian, crystal momentum is a good quantum number and optical transitions remain vertical. The dominant changes introduced by the perturbation consist of small shifts in the energy gaps, lifetime broadenings and transition matrix elements. Since these changes are small, the corresponding changes in ϵ are also small and can be approximated by first derivatives of the unperturbed dielectric constant:

$$\Delta\epsilon = \epsilon(\omega,\chi) - \epsilon(\omega,0) = \left(\frac{\partial\epsilon}{\partial E_0}\frac{\partial E_0}{\partial\chi} + \frac{\partial\epsilon}{\partial\Gamma}\frac{\partial\Gamma}{\partial\chi} + \frac{\partial\epsilon}{\partial P}\frac{\partial P}{\partial\chi}\right)\Delta\chi, \quad (2)$$

where χ is the external perturbation and E_0, Γ and P are the transition energy, lifetime broadening and matrix element, at a given critical point in the Brillouin zone. These are called interband mechanisms, and describe the effects of most modulating parameters (χ). In contrast to other forms of modulation, the electric field ($\vec{F}$) introduces a perturbation potential $V = -e\vec{F}\cdot\vec{r}$ that destroys the translational symmetry of the unperturbed Hamiltonian, H_0. This loss of translational periodicity results in a second, intraband,

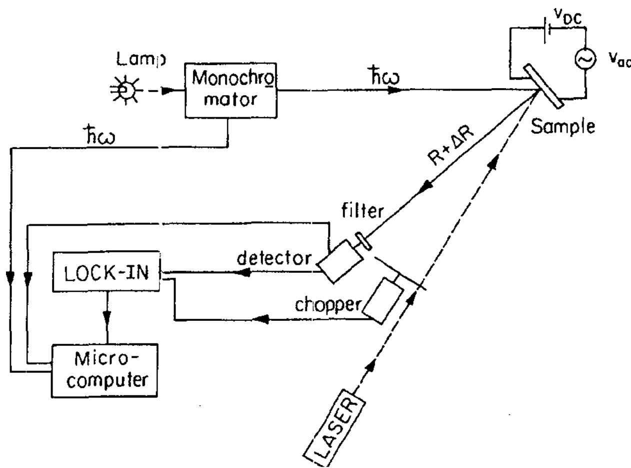

Figure 2: Typical experimental arrangement of a photoreflectance or electroreflectance experiment.

modulating mechanism. Here the field accelerates the electron in $\vec{k}$-space ($\hbar\dot{\vec{k}} = -e\vec{F}$) within a given band. This process introduces changes in ϵ that cannot be expressed in terms of first derivatives. The electric field also produces Stark shifts in transition energies, lifetimes and matrix elements that lead to first derivative changes in ϵ such as those given by eq. (2). However, for unconfined Bloch states such interband terms are negligible when compared to the intraband contributions to $\Delta\epsilon$ [4]. Low-field electroreflectance (ER) spectra are obtained when both mechanisms can be treated in first-order perturbation theory i.e., in a field regime in which an expansion to lowest order can be made in the ratio of two characteristic energies: one of the perturbation and another (much larger) of the system. For the interband mechanisms, the system energy is the interband energy separation (E_0) while the perturbation energy can be taken as the potential drop across one unit cell ($-eFa$). The condition for a perturbation treatment for this mechanism is, thus:

$$eFa \ll E_0. \tag{3}$$

The analogous energies for the intraband mechanism are less obvious, but the condition for validity of a perturbation expansion can be expressed by requiring that the average energy per particle gained by acceleration from the external field in the interval between collisions ($\tau \sim \hbar/2\Gamma$) be much less than the lifetime broadening of the Bloch state ($\sim \Gamma$). This can be quantitatively expressed as[4] :

$$\hbar\Omega \ll \Gamma, \tag{4}$$

where:

$$\hbar\Omega = \left(\frac{e^2F^2\hbar^2}{8\mu_{\|}}\right)^{\frac{1}{3}}, \tag{5}$$

and $\mu_{\|}$ is the reduced effective mass along the field direction. In this case, $\hbar\Omega$ and Γ are the perturbation and system energies to be compared.

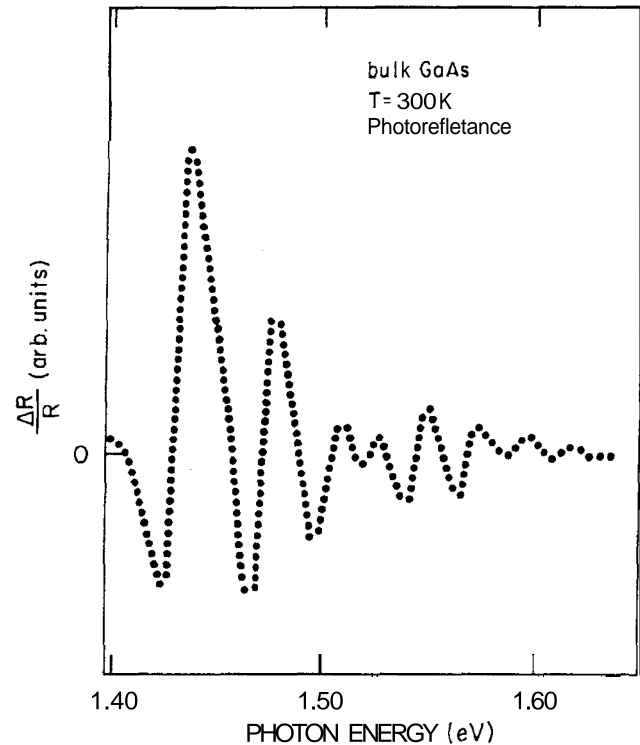

Figure 3: Photoreflectance spectrum of bulk GaAs showing FKO's associated with the direct absorption edge. From ref. [18].

In bulk semiconductors where $E_0 \sim 1$ eV and a ~ 6 Å, a violation of eq. (3) would require fields of such large magnitude ($F \geq 10^7$ V/cm) that a first-order perturbation expansion is always valid for the interband term. Fields that violate eq. (3) produce changes in the band structure of the material and the transitions between these altered states cannot be treated with the usual critical-point approach. We shall discuss these states further in section IV.2. It is possible to violate the condition of eq. (4) while maintaining that of eq. (3). This is specially true for the fundamental absorption edge in the case of direct gap materials. On the other hand, Γ increases rapidly with increasing energy so eq. (4) is almost always satisfied for higher transitions. This intermediate-field regime is dominated by the intraband mechanism. In the neighborhood of critical points the problem can be treated in the effective mass approximation. This treatment yields an exponential tail below the gap and a series of damped oscillations above it. When $\hbar\Omega > 3\Gamma$ these oscillations acquire a simple analytic form given by[17] :

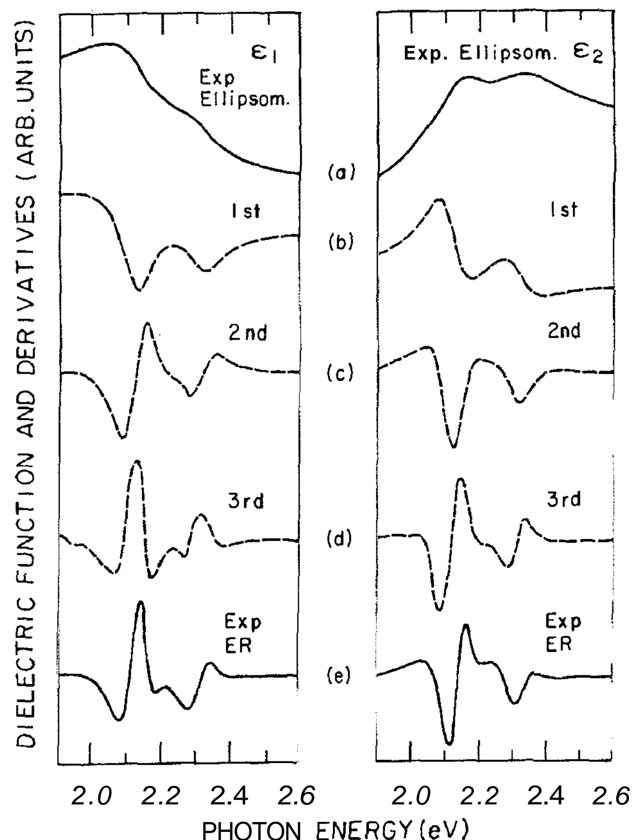

Figure 4: Real and imaginary parts of the dielectric constant from ellypsometric measurements, (a) and their derivatives numerically calculated, (b) - (d). In (e) the values of ϵ_1 and ϵ_2 ohtained from low-field electroreflectance are shown. From ref.[21].

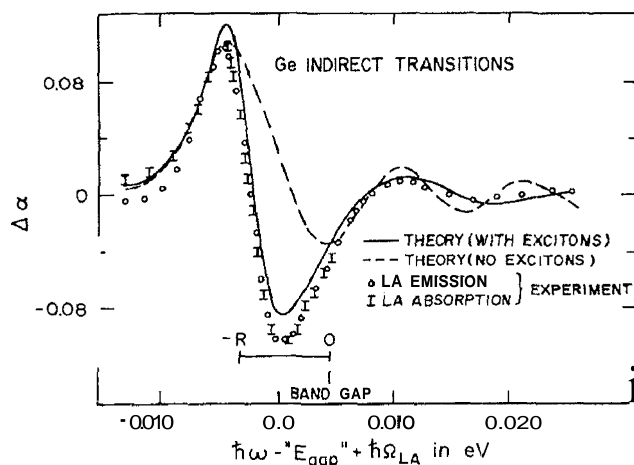

Figure 5: Comparison between experimental (open circles) and theoretical electroabsorption lineshapes for the indirect threshold in Ge after ref.[23]. The continuous (dashed) curve is a calculation which includes (does not include) excitonic interactions.

$$\hbar\omega_n = \hbar\Omega X_n + E_0 \qquad (n = 1, 2, ...), \qquad (6)$$

with:

$$X_n = \left[\frac{3\pi}{2}(n-\alpha)\right]^{\frac{2}{3}}, \qquad (7)$$

where the integer n numbers the alternating maxima and minima sequentially from the exponential tail and the value of α depends on the dimensionality of the critical point ($\alpha = 1/2$ for a $3D - M_0$). These Franz-Keldysh oscillations (FKO's) constitute an unmistakable signature of the intermediate-field regime. Fig. 3 sliows a representative example of this regime. There, the rooni temperature ER spectrum of GaAs around the direct absorption edge is shown (from ref.[18]). The oscillations for $\hbar\omega > E_0$ show beats due to the interferente of two sets of oscillations with different periodicity due to transitions between heavy and light holes to the conduction band.

Finally, when both eqs. (3) and (4) are satisfied, we are in the low-field regime, where the interband mechanism dominates. Here, the perturbation yields[4,5,19,20] :

$$\Delta\epsilon = \epsilon(\omega, F) - \epsilon(\omega, 0) = \frac{e^2\hbar F^2}{24(\hbar\omega)^2\mu_{\parallel}}\frac{\partial^3}{\partial\omega^3}[\omega^2\epsilon(\omega, 0)], \qquad (8)$$

where $\epsilon(\omega, 0)$ is the unperturbed dielectric constant and w the photon energy. The experimental lineshape can be obtained by substituting this expression for Aw into eq. (1). Thus, both $\Delta\epsilon$ and the experimental lineshapes ($\Delta R/R$ or $\Delta T/T$) are independent of the electric field and their peak intensity scales quadratically with it. These two characteristics can be used as identifying features of the low-field regime. When the fields are generated by a Schottky barrier at the semiconductor surface tliis quadratic dependence on $\vec{F}$ is translated into a linear dependence on the barrier potential (V_B) i.e., $\Delta R/R \propto F^2 \propto V_B$, and the lineshape is invariant when V_B is changed. This is a sure signature of the low-field regime[4]. As a rule-of-thumb, this regime is almost always achieved for $\Delta R/R \leq 10^{-4}$. A dramatic verification of the third derivative lineshape is shown in Fig. 4, where the values of $\Delta\epsilon_1$ and $\Delta\epsilon_2$ obtained from electroreflectance spectra [using eq. (I) and Kramers-Kronig analysis] of the E_1 and $E_1 +$ A, transitions in Ge [lowest curves, (e)] are compared to numerically calculated third derivative of these functions, measured directly by high resolution ellipsometry [second lowest curves, (*d*)][21]. This figure (comparing the lowest and uppermost curves) also illustrates the fact that the third derivative nature of low-field electroreflectance enhances critical point behavior and suppresses uninteresting backgrounds, yielding a structure that is different from zero only in a narrow photon energy range around the critical point.

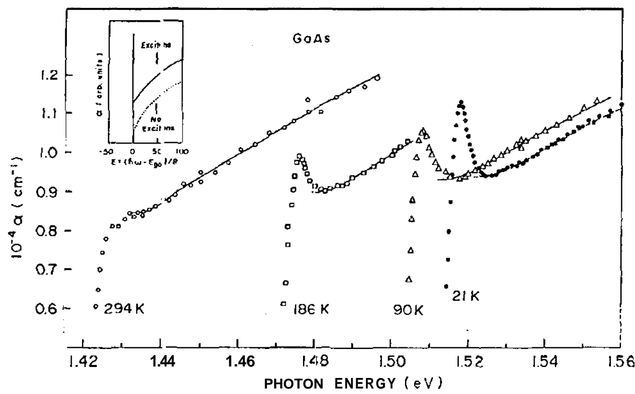

Figure 6: Absorption edge of GaAs at different temperatures after M. D. Sturge, Phys. Rev. 127, 768 (1962). Inset shows schematically the effect of electron-hole final-state interaction on suih an absorption edge.

In the vicinity of critical points, band energy differences can be substituted by a locally valid parabolic expansion. In this case, the dielectric function entering into eq. (8) can be approximated by[4,20]:

$$\epsilon(\omega,\Gamma) = A\Gamma^{-m}e^{i\phi}(\hbar\omega - E_0 + i\Gamma)^m, \tag{9}$$

where m $= -1/2, 0$ (logarithmic) and $1/2$ are the results valid for 1D, 2D and 3D critical points. In eq. (9) A is a constant that is proportional to the square of the transition matrix element and the phase factor ϕ depends on the type of singularity (M_0, M_1, M_2 or M_3)[4,20]. Motlulation lineshapes can now be obtained by substituting this locally valid form of ϵ into eq. (8) (intraband meihanism in low-field ER) or into eq. (2) (interband term in low- or intermediate-field ER or other form of rnodulation spectroscopy). Proceeding in this manner, and remembering the link between $\Delta R/R$ and $\Delta\epsilon$ given in eq. (1), experimental lineshapes obtained in low field ER can be fitted by expressions of the type:

$$\frac{\Delta R}{R} = Re\left\{\frac{Ce^{i\theta}}{[(\hbar\omega - E_0) + i\Gamma]^n}\right\}, \tag{10}$$

with $n = 7/2, 3$ or 5/2 for 1D, 2D or 3D critical points. Values of E_0 and Γ are easily obtained from these experimental lineshapes. Eq. (9) is valid for unconfined carriers in a situation in which final state electron-hole interaction is neglected. In physical situations where this picture applies, additional information about the dimensionality and singularity type (M_0, M_1, M_2 or M3) can be obtained from the values of m and θ obtained from fitting experimental lineshapes with eq. (9). This information is, however, more uncertain since field inhomogeneities and final state interactions produce drastic alterations in the values of these parameters[4].

111.2 Final-State Electron-Hole Interactions (Bulk Semiconductors)

Final-state electron-hole interaction (excitons) alters the one-electron picture described above. A general discussion of this subject is given by Dow[22]. Closed form solutions cannot be obtained even in the simplest of cases. Numerical calculations for direct and indirect M_0 absorption edges give a good description of experimental results for low- and intermediate-fields. A good example of this is the calculation of Weinstein, Dow and Lao[23] for tlie indirect electroabsorption of Ge (Fig. 5). The solid curve representing this calculation correctly describes the absorption edge and the FKO's occurring at higher photon energies while the dotted curve (calculation without excitons) gives a poor description of tlie data and only reproduces the higher FKO's. Figure 5 illustrates that even when the electron and hole are strongly correlated, intermediate fields still produce Franz-Keldysh oscillations. Surprisingly enough, the period of the correlated and uncorrelated cases is almost the same for n $\geq$ 3 (the first few oscillations have shorter periods in the excitonic case), when the asymptotic expansion leading to eqs. (6) and (7) is valid[17,22,23]

In the weak field limit it is sometimes possible to find simple asymptotic expressions for hydrogenic excitons derived from the lowest direct M_0 transition[5,22,24]. When the exciton concentrates most of the oscillator strength and its lifetime broadening is small enough, so that its absorption line is well separated from the band-to-band continuum, its contribution to the dielectric constant can be obtained from eq. (9) by setting[5,24] $m = -1$. In this case, the interband mechanism is the correct one since the exciton is a neutral entity and is, therefore, not accelerated by the field. Hence experimental lineshapes would be obtained by inserting the dielectric constant of eq. (9) with m $= -1$ into eq. (2), which leads to a $\Delta R/R$ of the general form as that given in eq. (10) with n = 2. In this case E_0 would be the band-edge energy minus the exciton Rydberg and Γ the lifetime broadening of the hydrogenic exciton. In addition to generating bound states in the forbidden gap, the Coulomb electron-hole correlation greatly enhances the absorption cross section for photon energies above the gap[22], as shown schematically in the inset of Fig. 6. So, when Γ is large and the excitonic line is not well resolved from the enhanced continuum, the shape of the absorption edge changes from a square root ($\alpha \propto \sqrt{\hbar\omega - E_0}$) to a step-like function characteristic of a $2D - M_0$ singularity. This is illustrated by Fig. 6, where the absorption spectra of GaAs taken at different temperatures are displayed. As the temperature decreases so does Γ, and the atomic-like Lorentzian absorption of the exciton becames more marked and better separated from the continuum. However, the enhanced absorption and

step-like behavior of the latter can be observed at all temperatures. Hence, for the electric-field modulated absorption (or reflectivity), eq. (10) with n = 3 (third-derivative lineshape of a $2DM_0$ singularity) also will fit the data in some cases where excitonic effects are important. It is only in extreme cases that it can be decided by purely physical arguments whether this clioice is better or worse than n = 2 (first derivative of a single Lorentzian contribution by an isolated hyclrogenic exciton). In an intermediate case the linesliape will be well reproduced by both choices, which will yield the same value of E_0[5,24]. The value of Γ, however, is more dependent on our choice of n as are the other two adjustable parameters (C and θ) in eq. (10). Therefore, when trying to ascribe physical significance to C, θ and sometimes even Γ, care must be taken to ascertain that our choice of n really describes the physical conditions of the experiment.

The above discussion can be summarized by saying that, if we are in the low-field limit, eq. (10) is useful in all practical situations that involve bulk semiconductors (whether excitonic effects are important or not). Use of this lineshape to fit experimental spectra yields good values of transition energies (E_0) and, in most cases, lifetime broadenings. When extreme care is taken to fit the choice of n to the actual physical situation, information about singularity type also can be obtained from the phase factor (8). The amplitude C is generally of use when testing selection rules, comparing lines arising for different transitions in the same spectrum or following the dependence of this parameter in a given line as a function of an external perturbation (stress, external-applied fields, etc.)[25].

111.3 Applications to Semiconductor Microstructures

When applying the results described above to semiconductor microstructures, care must be taken to ascertain that the assumptions that led to the lineshape equations such as eqs. (8) to (10) are still valid. In some of these structures the carriers are confined in the direction of the modulating field. Such is the case of single qnantum wells (SQW) or multiple quantum wells (MQW), separated by large barrier regions, with the modulating field along the growth axis. In these cases, carriers cannot be accelerated by the field and the intraband term, which leads to third-derivative lineshapes, does not contribute to $\Delta\epsilon$. Although there have been reports to the effect that experimental lineshapes in MQW's are well described by TDLS of $2D$-critical points[26–29], this may not be physically meaningful. It is true that the joint density of one-electron states is a step function ($2D$ – Mo), but since the field is applied along the direction of confinement it does not accelerate the carriers (intraband term) and produces no third-derivative terms in **Ar.** This is compounded by strong evidence that in tliese structures excitonic interactions are of great importance even at room temperature[30–34]. Thus, low-field ER from these confined systems should produce first derivative lineshapes (FDLS), with Ar given by eq. (2). In applying this equation, however, one must first determine the appropriate form of ϵ. The subject was recently discussed by Glembocki and Shanabrook[35,36], who study the ER and PR spectra of some MQW's of AlGaAs/GaAs at temperatures ranging from 6 K to room temperature. The lowest temperature PR spectra are compared to pliotoluminescence excitation (PLE) results. Tliis comparison shows that the PR line arises from electric-field modulation of an excitonic transition and that both its transition energy and lifetime broadening are well described, at low temperatures, by a first-derivative lineshape of a Lorentzian (hydrogenic) excitonic contribution to E, i.e., eq. (10) with n = 2. For temperatures $T \geq 150K$, however, FDLS of a dielectric function with a Gaussian profile gives better fit to tlie data[36]. The Gaussian nature of excitonic absorption lines may arise under a variety of conditions, including strong exciton-phonon coupling (as in high temperatures) inhomogeneous perturbations and rough interfaces[9]. It is to be noted, however, that these lines are also well reproduced by TDLS of a 2D-critical point [eq. (10) with n = 3]. This fit yields the same value of E_0 as the FDLS of a Gaussian ϵ_2, albeit considerably different values of Γ. The authors of references [35] and [36] believe this to be fortuitous. However, the evidence in favor of Gaussian excitonic absorption is mostly empirical. Aspnes[37] suggests that the only prerequisite for obtaining TDLS may be that the carrier (electron or hole) acceleration by the field has actual physical meaning. In a QW, motion along tlie field (z) direction corresponds to transitions between subbands. When high temperatures or rough interfaces make intersubband separations of the same order of lifetime broadenings, the field, however weak, may easily mix wavefunctions of different subbands which, in semiclassical terms, has the effects of acceleration along the field direction. This situation is far more common tlian can be at first imagined if instead of thinking about electrons, we focus our attention on heavy holes, which have larger effective masses and are subject to shallower confining potentials in most microstructures[38]. In this case, the appropriateness of using TDLS of 2D singularities (since the electrons are still confined in the z-direction) gains physical significance. Another situation in which TDLS might be appropriate is when there is sufficient overlap between the wavefunctions of carriers confined in different QW's, so that field-induced tunneling between wells is possible. The degree of overlap is determined by the width of the barriers, the depth of the QW's and the order of the confined level; con-

fined states of large quantum numbers lie closer to the edge of the quantum well, producing larger overlap and larger lifetime broadenings. An extreme case would be that of a true superlattice, when confined levels evolve into continuous minibands of width $\Delta \sim 10 - 50$ meV $\ll \Gamma$. In these cases the states are truly 3D, but with a mass considerably larger along the z-direction, which might lead to TDLS of approximately 2D-critical points even in the presence of excitonic effects.

Another point under discussion is whether in such systems, full understanding of the spectrum can be achieved by derivatives of locally-valid dielectric functions based on expansions in terms of localized van Hove singularities, especially when final-state electron-hole correlations are taken into account. This picture may break down when these singularities have an energy spacing smaller than, or of the order of, some other significant energies in the problem, such as miniband energy spread (Δ), the exciton binding energy (E,,,), the lifetime broadening of the one-electron state (Γ) or the typical energy that a carrier may gain from the accelerating electric field ($\hbar\Omega$). Recent calculations for SQW's show that even when tunneling along the field direction is not possible, intersubband mixing and subband dispersion in the xy-plane (Ito the field and confining directions) produce features in the ER spectra that cannot be predicted by a critical point analysis[39].

The discussion above shows that the question on the appropriate lineshape to be used in fitting experimental spectrs of electric field modulated reflection or absorption is both complex and not completely settled. As a rule-of-thumb, TDLS of 2D singularities [eq. (10) with n = 3] seem to give good overall-fits of frequently encountered situations. The same can be said of FDLS of Gaussian profiles. Both fittings give reliable values of E_0, but in order to ascribe physical significance to the other parameters resulting from the fit, a good understanding of the actual physical situation is required.

IV. Recent Results

IV.1. Low Field Regime

In the conditions of low fields [eqs. (3) and (4)], structures in the photomodulated spectra of QW's, MQW's and superlattices originate in transitions between hole and electron subbands. These subbands can generally be calculated (in direct band-gap materials) with variations of a simple Kronig-Penney model[38] based on the fact that the different gaps of the constituent materials generate, for a free carrier in the effective-mass approximation, a periodic square well structure. To describe this potential the band alignments on both sides of the heterojunction must be known. Hence, one of the most important results of this type of spertroscopy is to determine the band alignments in different heterojunctions. Another important question is determining the degree of spread of the states produced by this periodic potential as a function of coupling between neighboring quantum wells. Finally, the validity of this simple description might be questioned, especially in cases where the bulk constituents do not have direct gaps. Modulation spectroscopy has contributed, and still contributes, to find answers to these questions. In what follows we illustrate this using as examples photo and electromodulated reflection and absorption work performed in our laboratories in two strained-layer systems: InGaAs/GaAs and Ge/Si quantum wells and superlattices.

IV.1.1 The $In_xGa_{1-x}As/GaAs$ System

Strained-layer $In_xGa_{1-x}As/GaAs$ superlattices have been extensively studied by optical techniques[40]. In this system, the electronic states of interest are totally or partially confined within the alloy material. Hence, the large portions of the sample that constitute the substrate, buffer and capping layers are made up of GaAs and are transparent in the photon energy range of interest. This allows spectroscopic measurements to be performed in transmission, rather than in reflection, which has the advantage that all the contributions to the observed spectra come from the region of the sample containing the microstructures under study, since the sample became opaque when the absorption edge of GaAs is reached. On the negative side, the confined states are broadened by such effects as the random potential of the InGaAs alloy and the inherently rougher interfaces which occur in strained-layer superlattices, even in the absence of strain relaxation. Even so, the study of direct[41] and photomodulated transmission[8] has given important insights into the electronic properties of microstructures based on this type of heterojunctions.

(i) Band Alignment

One of the most important questions about this system is the value of the offset parameter Q, defined as

$$Q = \frac{\Delta E_c}{\Delta E_c + \Delta E_v^{HH}}, \qquad (11)$$

where ΔE_c and ΔE_v^{HH} are the conduction and heavy hole valence band discontinuities, respectively. The large splitting between light- and heavy-hole valence bands produced by biaxial strain results in a different potential profile for each type of carrier. For some values of Q($Q \geq 0.6$) it is possible to confine light holes in the GaAs layers while both electrons and heavy holes are confined in the lower energy gap alloy layers. Accurate determination of this parameter, however, proved to be a difficult task. Light scattering experiments[42] suggested $Q \simeq 0.4$, while other optical techniques yielded values of Q between 0.6 and 0.8[43-49]. In an attempt to reconcile this diversity of values, Joyce et al.[50] suggested that the value of Q

might depend on the Indium molar fraction, x, taking values of Q $\simeq$ 0.4 for low molar fractions and increasing to Q $\simeq$ 0.8 as molar fraction increased. This assumption received some support from PR measurements[51] performed on two $In_xGa_{1-x}As/GaAs$ samples of x = 0.19 and x = 0.45. More recently, Vázquez-López et al.[8] performed a systematic study of this system using photomodulated reflectance and transmission. In their study they used a collection of $In_xGa_{1-x}As/GaAs$ microstructures that included superlattices, as well as inultiple and single quantum wells with molar fractions ranging from x = 0.12 to x = 0.22. Fig. 7 shows representative photomodulated transmission spectra of two samples of this series. Although FDLS of Gaussian profile gives the best fit to the data in most cases, TDLS of 2D singularities also fit the data well, as shown by the solid line in Fig. 7(a) and (b). The insets in these figures show the transition energies obtained from fitting the spectra (horizontal straight lines) and the energies calculated[8,38,41] for the parity-allowed transitions as a function of the offset parameter Q. The correct value for this parameter should be that in which the calculated and experimental lines intersect one another. This point is quite well identified in the inset of Fig. 7(b) where the two calculated lines for the first light-hole transition and the second heavy-hole transition simultaneously intersect the second experimental line. By pursuing this procedure systematically with samples of different well and barrier widths as well as different molar fractions it was found that a single value of the offset parameter (Q $\simeq 0.60 \pm 0.03$) is obtained, with no appreciable dependence of Q on x. The value of Q thus obtained corresponds to a situation in which the light holes are weakly confined into the GaAs layer. The confinement potential is, however, smaller than the exciton binding energy. This is linked to the fact that the light hole to conduction band transition [L(11)] appears always in the spectra. This sets un upper limit for the offset parameter (Q < 0.7), since for large enough values of Q the light hole would be effectively confined in the GaAs layers with consequent vanishing overlap between its wavefunction and that of the electron (confined in the alloy layer) which, in turn, would mean the disappearance of the L(11) line from the optical spectra. Lower limits of Q(Q $\geq$ 0.5) are also set by the presence or absence of certain spectral lines, such as the H(22) line in Fig. 7(a) and minizone edge (see below) transitions in other samples [Figs. 8 and 9]. The overall consistency of the results obtained for all samples yield Q $\simeq$ 0.60 as the best estimative for this parameter.

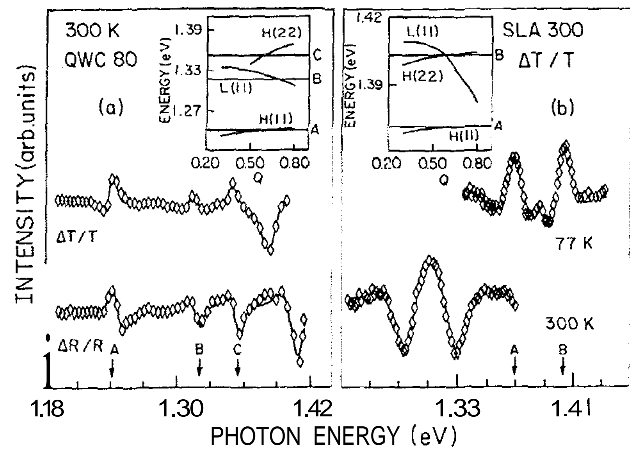

Figure 7: Photomodulated transmission spectra of (a) a SQW of $In_{0.22}Ga_{0.78}As$ in GaAs and (b) a (100 Å/200 Å) MQW of $In_{0.12}Ga_{0.88}As/GaAs$. Insets show a comparison between calculated (curves) and experimental (straight lines) transition energies.

(ii) Miniband Dispersion

Another issue that was clarified by these studies was the extent of miniband dispersion in InGaAs/GaAs superlattices and the possibility of resolving spectral features arising from different singular points in the mini-Brillouin zone. The coupling between quantum wells in a superlattice turns the discrete levels into continuous bands. For large enough dispersion, we might expect the absorption of light due to transitions between hole and electron minibands to exhibit sharp structures only in the vicinity of van Kove singularities of the joint density of states. In a superlattice of period d, transitions associated with the bulk E_0 structure have singularities at points $k_z = 0$ (r-point in the minizone) or $k_z = \pi/d$ (π-point in the minizone) with both $k_x = k_y = 0$. At these points the joint density of states has maxima (minima) as a function of k_z resulting in M_0 (M_1)-type singularities[52]. Final-state Coulomb interactions between electron and holes have different effects on each type of singularities. As previously discussed, an M_0 exciton enhances the oscillator strength of this transition, producing a sharp hydrogenic absorption peak just below the absorption edge. For an M_1 singularity, the Coulomb interaction also redistributes oscillator strength but does not result in a hydrogenic peak as in the M_0 case. Thus, peaks in the modulation spectra at M_1 singularities are expected to be much weaker than their M_0 counterpart[52]. Even

worse, since the energy separation between both singularities (A) might be of the order of the binding energy of the M_0 hydrogenic exciton (E_{exc}) the redistribution of oscillator strength produced by the latter might obliterate the contribution of the M_1 singularity to the absorption spectrum (i.e., wavefunction from the whole miniband might enter the formation of a single hydrogenic exciton). Even if Coulomb interactions were not important, these two singularities could not be resolved if A was not much larger than the lifetime broadening of one-electron states (Γ). Hence, the observability of two distinct spectral lines in the modulated absorption spectra, arising from the two singular points Γ and π on the minizone, depends on A being larger than Γ and $|E_{exc}|$. Typical values of these quantities are $\Gamma \sim 1-7$ meV and $|E_{exc}| \sim 10$ meV. Hence, we would expect to see manifestations of the miniband dispersion in the optical spectra for $A \geq 20$ meV. Such manifestations were reported by Shen et al.[53] for AlGaAs/GaAs superlattices and by Ribeiro et al.[9] and Vázquez-López et al.[8] for InGaAs/GaAs superlattices.

In figure 8(a) the 77 K photomodulated transmission spectrum of a 100 Å-period superlattice made up of equal layer thickness of $In_{0.16}Ga_{0.84}As$ and GaAs is shown (ref [8]). The solid line represents a fitting with an FDLS of a Gaussian absorption profile. Three transitions [arrows in Fig 8(a)] are needed to fit the spectra: two strong ones (A and C) and a weaker one (B) to account for the shoulder in the higher energy side of line A. The necessity of including the latter is illustrated by the dashed line, which represents a fit where this weak transition is omitted. The inset in Fig. 8(a) shows the parity-allowed transitions calculated as a function of the offset parameter (curves) and the transition energies (straight horizontal lines) obtained from fitting our spectrum. The electron and heavy-hole minibands, from which these transitions were calculated (Q = 0.60), are shown in Fig. 8(b). The stronger peaks in the spectrum (A and C) are assigned to the M_0 singularity at the zone center due to transitions from both light- and heavy-hole valence-band states to the only electron miniband. Line B appears in a region where no transitions occur at the center of the minizone. Its position is in the neighborhood of the (M_1) saddle point singularity occurring at the edge of the minizone (π-point). A similar shoulder is observed in the photoreflectance spectrum of a 00 Å-period AlGaAs/GaAs superlattice by Shen et al.[53] and is also attributed to a transition at the π-point of the minizone. These authors point out that the modulation produced by the electric field at the Γ- and π-points has opposite phase. Our fittings result in a phase for line B which is opposite to those of lines A and C. Also, the zone center M_0 and the zone edge M_1 singularities should be separated by an energy of **33** meV [Fig. 8(b)]. The energy separation of our spectral features is 25 ± 4 meV. This agreement is very good when considering that the calculated energy separation does not take into account excitonic effects and that this separation is very sensitive to small fluctuations in the superlattice period d [shaded area in inset of Fig. 8(a)].

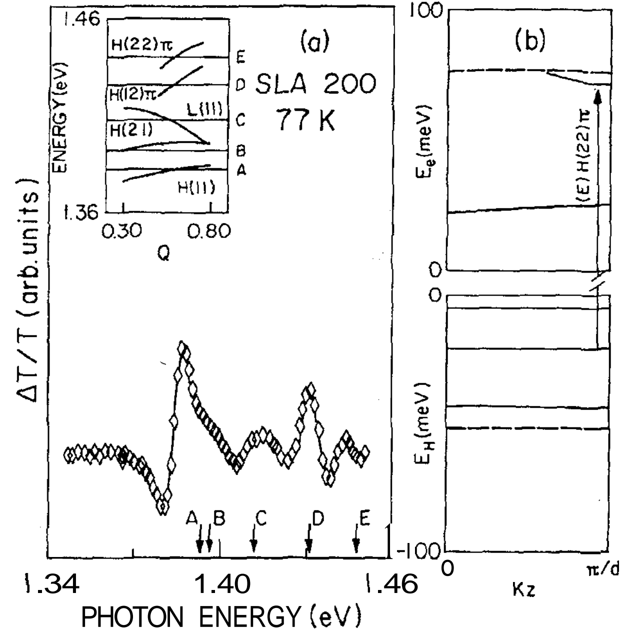

Figure 8: (a) Photomodulated transmission of a 100 Å period $In_{0.16}Ga_{0.84}As/GaAs$ superlattice with equal alloy/GaAs thickness and twenty repetitions; (b) Miniband dispersion calculated for $Q = 0.60$.

Another example is given in Fig. 9(a) which shows the $\Delta T/T$ spectrum of a 200 Å- period superlattice made up of equal layer thickness of $In_{0.12}Ga_{0.88}As$ and GaAs at 77K. The calculated minibands (Q = 0.59) are shown in Fig. 9(b). The spectrum is fitted (continuous-line) in the manner previously described with five transitions, labelled A, B, C, D, and E, in order of increasing energy indicated by arrows in Fig. 9(a). These are shown in the inset of Fig. 9(a) as horizontal straight lines, while the curves represent the energies for the various possible transitions arising from the theoretical miniband scheme [Fig. 9(b)] as a function of Q. The assignment of lines A to C as well the choice of Q = 0.59 for the offset parameter are discussed in ref. [8]. Here we shall be concerned only with the assignment of lines D and E. They are both relatively strong and well defined lines that cannot be attributed to any allowed or forbidden zone-center transitions. Fig. 9(b) shows that the second electron miniband is strongly dispersive, having a minimum at the minizone edge and increasing its energy with decreasing wavevector in such a way that it merges into the continuum before it reaches the minizone center. Since the first and second heavy-hole minibands are virtually dispersionless, transitions from these bands into the second conduction miniband at the zone edge would give rise to M_0 singularities in the joint density of states. In contrast, these same transitions at the zone center should not contribute to the

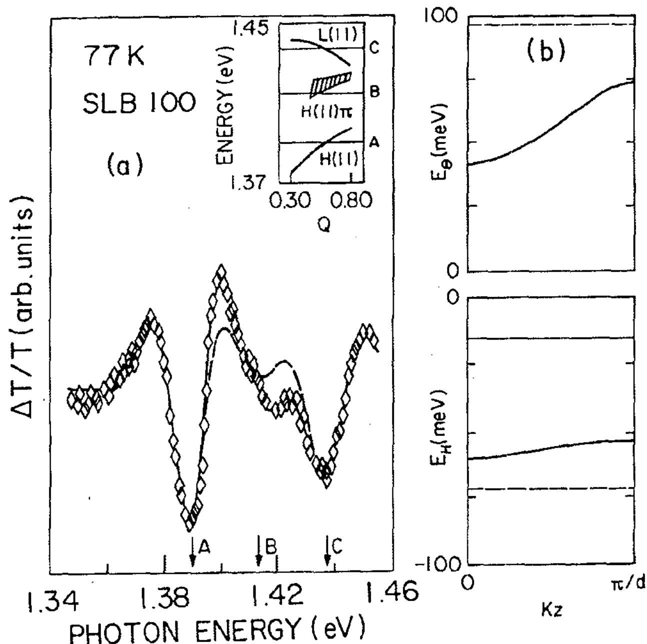

Figure 9: (a) Photomodulated transmission of a 200 Å period $In_{0.12}Ga_{0.88}As/GaAs$ superlattice with equal thickness alloy and GaAs layers and twenty repetition; (b) Miniband dispersion calculated for $Q = 0.59$.

absorption because of the M_1 character of the singularity and, even more important, because the electron state is unconfined [Fig. 9(b)] at this point of the minizone. Identifying lines D and E in the $\Delta T/T$ spectrum of their sample with these two zone-edge transitions is also coherent from the energy point of view, as shown in the inset of Fig. 9(a).

Evidence of distinct spectral features due to miniband dispersion has also been reported in the ER spectra of Ge/Ge_xSi_{1-x} superlattices[14] (to be discussed in the following section). Here the much deeper quantum wells in the Ge layers produce a series of subbands with quantum numbers ranging from $n = 1$ up to $n = 4$. The miniband width increases from one or two meV for the lowest confined subband to $\Delta \simeq 50$ meV for the uppermost electron miniband. In consonance with our previous discussion, a (Γ, π)-doublet (lines G and H in Fig. 10) can be associated with the $n = 4$ heavy-hole transition, but no such structures are resolved for the transitions with lower subband index.

The experimental evidence discussed above shows that miniband dispersion can cause distinct spectral features associated with the two critical points (Γ and π) in the mini-Brillouin zone when Δ is sufficiently large ($\Delta \gg |E_{exc}|$, $\Delta \gg \Gamma$). When this is not so, the effects of miniband dispersion will manifest themselves in more subtle ways and interpretations in terms of van Hove singularities are not appropriate. Recent calculations[39] suggest that not only the dispersion of the minibands along the superlattice axis influences the spectral lineshapes, but also the in-plane dispersion may contribute significantly to the number and relative intensities of the lines appearing in the ER spectrum. So, again, extreme care must be exercised when attributing lines in experimental data to a given type of singularity in the band structure of superlattices.

IV.1.2 The Ge/Si System

The pseudomorphic, strained layer epitaxy of Si/Ge superlattices has attracted much attention in the last years both from the technological and fundamental points of view[54-58]. However, the description of the electronic states in these materials is not simple. It is well known that the built-in strain present in this system, due to the lattice mismatch between bulk Si and Ge, drastically alters the band edge positions[59]. First principles ab initio calculations[60,61] of the relative positions of band edges (band offset) predict an almost constant alignment between the average valence bands of commensurate grown Si and Ge (the average valence band of Ge being always ~ 0.54 eV above that of Si), which does not depend on the built-in strain in each layer. They suggest a linear interpolation of this band offset for superlattices composed of alternating layers of Si or Ge with Ge_xSi_{1-x} alloys. Their results were used by People and Bean[62] to explain earlier observations of mobility enhancement in modulation doped Si/Ge_xSi_{1-x} samples[63,64] and confirmed by recent core-level photoemission experiments[65] in Si/Ge heterojunctions. However, optical techniques[41] are known to determine band offsets with less uncertainty when compared with mobility enhancement or photoemission experiments.

For the $Ge/Ge_{0.7}Si_{0.3}$ grown on Ge (001) the calculations of refs. [60] and [61] predict a type I alignment at the Brillouin zone center with the local minimum of the bulk-Ge conduction band below that of the bulk alloy and the valence-band maximum of bulk Ge above the strain-split valence-band maximum of the alloy. Since the direct gap difference of the two constituent materials is high (~ 1 eV), we might expect several conduction-band confined states at the Brillouin zone center. In this case, confinement energies of the same order of, or even higher than, the bulk-Ge energy gap at the Γ-point are possible. Hence, band non-parabolicities[66] must be taken into account when calculating the energies of the confined states[67-70]. On the other hand, confinement by zone-center states may not fully describe the conduction-band states of these superlattices at the Γ-point because both materials have the absolute conduction-band minimum far from the zone center. This would make it necessary to adopt a more elaborate theoretical model[71] than the widely used scalar Kronig-Penney or Bastard two band model[72] in order to describe these states. These quantum-confined direct transitions have been previously reported in Si/Ge_xSi_{1-x} quantum wells[73,74] as well as in the Ge spacer layers separating adjacent

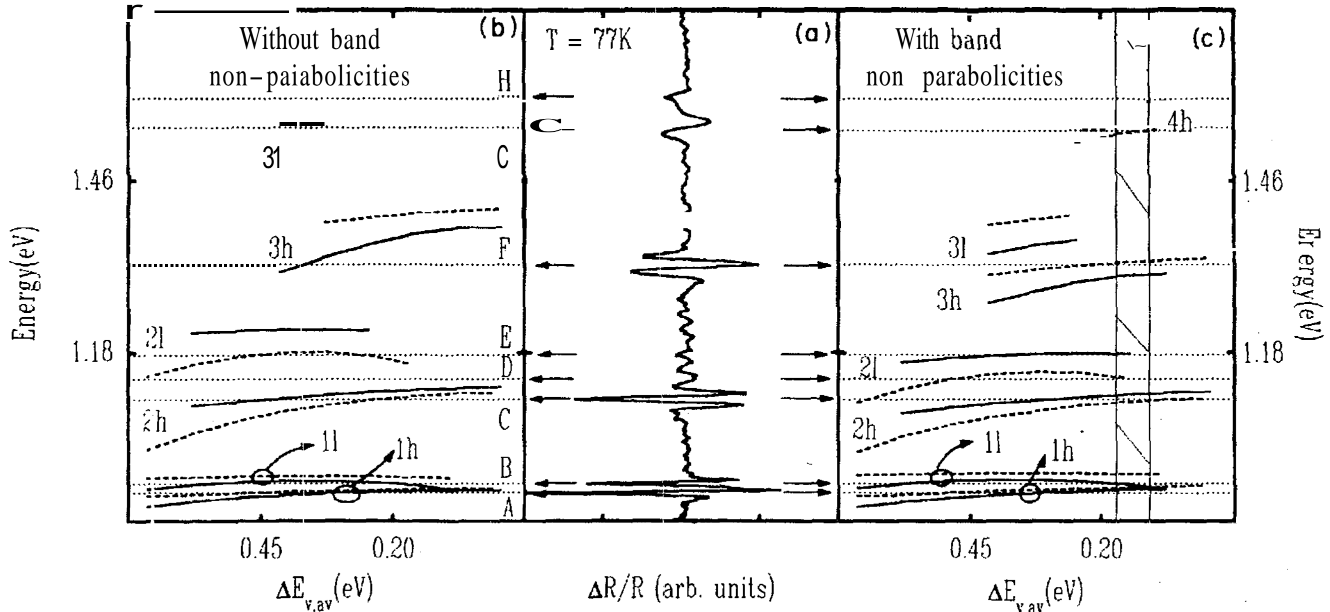

Figure 10: (a) Photoreflectance spectrum of a $Ge/Ge_{0.7}Si_{0.3}$ (1.11Å/ 32 Å) x 20 superlattice. Arrows indicate the transition energies obtained from a FDLS of a Gaussian absorption profile. Comparison with calculated minizone center (edge) transitions are given as continuous (dashed) curves in (b) with constant effective masses and (c) with energy dependent effective masses.

Si_nGe_m thin layer superlattices[75]. However, quantitative comparison between calculated and experimental energy transitions, where it was possible (ref. [74] and [75]), differs by as much as 110 meV.

A recent photoreflectance study performed on $Ge/Ge_{0.7}Si_{0.3}$ superlattices by Rodrigues, Cerdeira and Bean[14] shows that these discrepancies can be explained without invoking mixtures of bulk Γ, X and L states if band non-parabolicities are taken into account. Fig. 10(a) shows a representative PR spectrum in the photon energy region of 0.95 - 1.70 eV. The authors identify the lines in this spectral region (A to H in order of increasing energy)as originating in transitions between confined superlattice states derived from bulk Ge r-point states. The identification is made in a rnanner similar to that explained in section IV.1.1(i). First, a calculation is made with a simple scalar version of a Kronig-Penney[72] model, using zone-center bulk states and constant carrier masses, as a function of the discontinuity of the average valence bands (ΔE_v^{av}) [60]. The results of these calculations are shown in Fig. 10(b) as a solid (dashed) curves for parity allowed transitions at the minizone center (edge) while experimental transition energies are represented in this figure by horizontal dotted lines. Agreement between calculated and measured transition energies is poor, regardless of the value chosen for ΔE_v^{av}, for all but the lowest energy lines in the PR spectrum. The origin of these discrepancies (as well as those reported by other authors) can be understood if we notice that confinement energies in these systems can have values considerably larger than that of the E_0 transition in bulk Ge. This should produce strong dependence of the carrier effective mass on the confinement index n. Taking these non-parabolicities into account, Rodrigues et al.[14] used the same model to recalculate the transition energies. Now, excellent agreement is obtained for a band offset of $\Delta E_v^{av} = 0.14 \pm 0.03$ (Q = 0.73 ± 0.03), as can be seen in Fig. 10(c). Hence, the use of PR has demonstrated the validity of treating these transitions in terrns of bulk r-point bulk-Ge states, shown the importance of band non-parabolicities in the case of deep potential wells and deterrnined the band-offset parameter for the Ge/Ge_xSi_{1-x} interface.

The validity of using a simple Kronig-Penney type model in the Ge/Si system is the most striking of the results described above. Still, this was demonstrated for a superlattice with a relatively large period (d $\simeq$ 140 Å). The nagging question remains as to whether the same would be true for the very thin superlattices obtained by alternating layers of Si and Ge, each only a few monolayers thick[57]. Figure 11 shows ER spectra of three Ge_nSi_m superlattices, where n (m) is the number of monolayers of Ge (Si) in each period of (n+m)-thickness. Determination of the E_0 optical transition in these samples is not always easy. In thin samples, such as Ge_5Si_5 (upper curve in Fig. 11), interference patterns mask the ER line. However, using the method suggested by Garriga et al.[76] a good estimate of the transition energy is obtained. In thicker samples, as in

the $Ge_{16}Si_{16}$ (lower curve in Fig. 11), a strong ER line associated with defect formation appears just below the direct absorption and hinders the observation of the E_0 structure. The middle curve shows an ER spectrum (Ge_8Si_{12}) in which this structure is clearly observed. In this case the transition energy can be unambiguously obtained from a fitting with a TDLS for 2D singularity. The values thus obtained from these spectra coincide within $\simeq 0.1$ eV with the predictions of a non-parabolic three-band model. For the thinner sample this prediction also coincides with that of more sophisticated LMTO calculations[77]. These results suggest that the non-parabolic three-band model retains its predictive value for the direct gap even down to superlattices of only ten monolayers in thickness. Figure 11 also shows a complex of structures (delimited by the vertical solid and dashed lines) at higher photon energies. These can be associated with the E_1 transitions in the siiperlattice. No simple model has yet been developed to understand these structures[77]. In spite of the surprising result concerning the E_0 transitions in these siiperlattices, the full understanding of their ER spectra calls for further work.

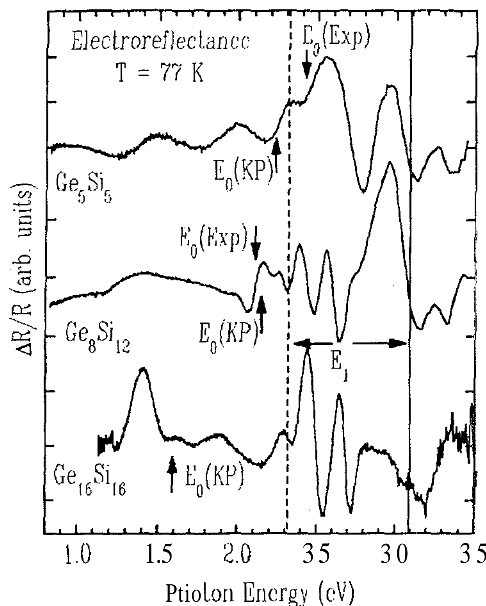

Figure 11: ER spectra of Ge_nSi_m superlattices. Arrows indicate the value of E_0 calculated with Kronig-Penney model [E_0(KP)] and those obtained from experiment. The shaded photon energy region contains structures related to bulk E_1 transitions.

IV.2 Intermediate and High-Field Regimes

So far we have Iimited our discussions to results obtained in the low-field regime, where the spectral features are interpreted in terms of intersubband transitions. As discussed in section 111, the absorption coefficient shows marked changes when fields exceed those imposed by the criteria of eqs. (3) and (4). In bulk semiconductors it would be difficult to obtain an electric field high enough that would take the problem into the high-field regime. Here the effective-mass approximation can be used and the eigenstates in the presence of the field are Airy functions, which are delocalized and have a continuous energy spectrum. Transitions between these eigenstates produce an absorption coefficient with an exponential tail at photon energies below the absorption edge and oscillations above it with periodicity given by eq. (6). This process was discussed in section 111.1 and is pictorically illustrated in Fig. 12(a). Our ideas about these effects must be revised when applied to semiconductor microstructures. The closer spacing between subbands and the smaller subband dispersion in semiconductor superlattices can create the conditions for achieving high-field regimes with moderate electric fields. Such conditions have allowed the observation of Stark-Wannier ladders in the photo-conductivity and electroreflectance spectra of $Al_xGa_{1-x}As/GaAs$ superlattices[78-82]. In these cases the intermediate-field regime proved to be more difficult to identify and was only recently reported by Cerdeira et al.[10]. On the other hand, this regime might take an entirely different form when only one type of carrier can be accelerated by the electric field, while the other is confined by the microstructure potential along the field direction. Such a situation, illustrated in Fig.12(b), would occur in the 2D-electron gases confined in modulation-doped heterojunctions or in the V-shaped potential of GaAs samples with Si-δ-doping, and might result in a quantum-confined version of the F'ranz-Keldysh effect. These two cases shall be discussed in the following two subsections. When studying these cases it must be kept in mind that the fields which alters the electronic wavefunctions are externally-applied dc-fields or the internal fields created by the microstructure (as in the 2DEG). The modulating ac-fields are small and constitute a perturbation on the dc-field.

IV.2.1. $In_xGa_{1-x}As/GaAs$ Superlattices

We already saw that the conditions for Franz-Keldysh oscillations are almost always satisfied in bulk direct-gap semiconductors. In order for these oscillations to appear in the spectrum, with the periodicity of eq. (6) (i.e., period proportional to $F^{2/3}$), two things are necessary: that the electric field be small according to the criterium of eq. (3) and that the effective mass approximation be valid. The first condition insures that the dominant mechanism of interaction between the field and the carrier is the intrahand acceleration by means of which it gains a typical energy of the order eFd (d is the period of the lattice along the field direction). The second is insured by requiring that, in gaining this energy, the carriers do not stray too far from the extrema, when a parabolic expansion of the

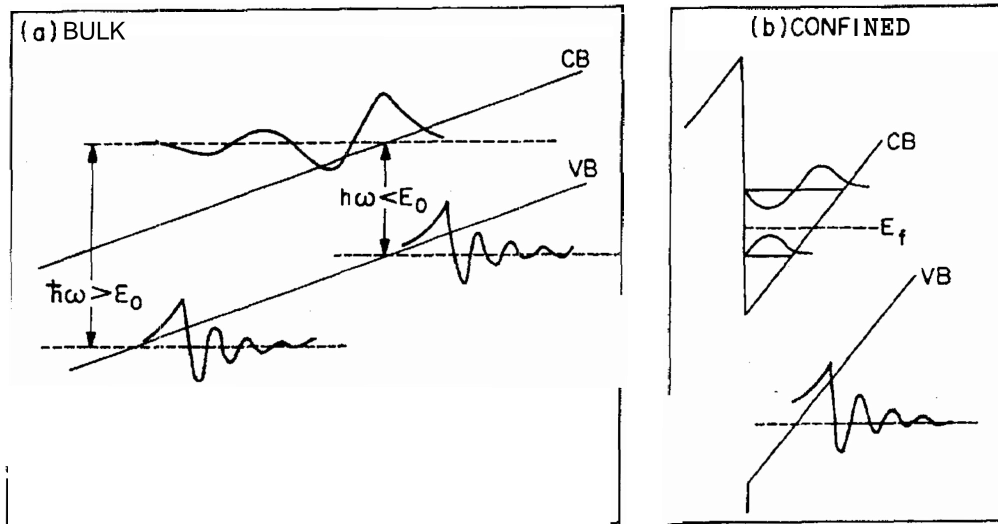

Figure 12: Schematic representation of the optical transitions that lead to the Franz-Keldysh effect in the absorption edge of a direct gap semiconductor in (a) bulk and (b) the space-charge region of a modulation doped heterojunction.

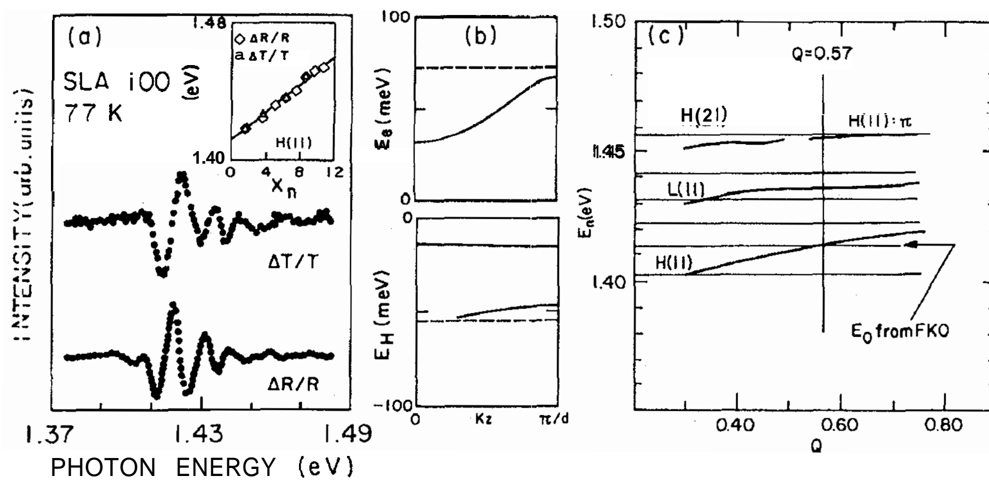

Figure 13: (a) Photomodulated reflection and transmission of an $In_{0.12}Ga_{0.88}As/GaAs$ superlattice of 100 Å period and equal alloy and barrier thicknesses. The inset shows a plot of the photon energy of the alternating maxima and minima in the spectra according to eq. (6) in the text; (b) dispersion of the only electron and the two hole minibands for a band offset parameter of $Q = 0.57$ and (c) a comparison between calculated transitions between these minibands (curves) and transition energies obtained from the spectra (horizontal straight lines) by fitting them with TDLS's.

energy band in terms of some effective mass is Iocally valid. This is more or less equivalent to requiring that the acceleration energy (eFd) be very small in terrns of the width of the energy band (A), i.e.:

$$f = \frac{eFd}{\Delta} \ll 1, \tag{1}$$

where the dimensionless quantity f is often referred to as the "effective electric field" . As f approaches unity, the wavefunction of the carrier becomes localized on a length scale λ E d/f. When this happens, the effective-mass approximation is no longer valid and the coupling between states in different unit cells along $\vec{F}$ decreases. Here a tight-binding approach is a better starting point for discussing the problem. For f > 1 these states become totally decoupled and the resulting regime is known as that of Stark-Wannier localization. The absorption coefficient in this case would show a series of equally spaced ($neFd$; n $= 0, \pm 1, \pm 2, ...$) peaks known as Stark-Wannier ladders (SWL's). Although the conditions for achieving this regime are difficult to meet in bulk serniconductors (d E $6\AA$, A $\sim$ 1 eV), in a superlattice both bandwidths and periods can be tailored to obtain f $\sim$ 0.1 at relatively modest fields (**F** $\sim 10^4 - 10^5$ V/cm). Following the first reports of SWL formation[81,82], the high-field regime in semiconductor superlattices has been studied with a variety of techniques by different authors[78,79,83]. The intermediate-field regime for these materials, however, has not been very well studied. To the best of our knowledge, the first report of FKO in a semiconductor superlattice is that of Cerdeira et al.[10]. These authors studied the photomodulated reflection and absorption spectra of an $In_xGa_{1-x}As/GaAs$ superlattice with a built-in field of **F** E 7 kV/cm and found an oscillatory structure, which can be unambiguously attributed to FKO's. Photomodulated reflection ($\Delta R/R$) and transmission spectra of this sarnple (d $= 100\AA$, $x = 0.12$) are displayed in Fig. 13(a), while the minibands of the superlattice are shown in Fig. 13(b). We first notice that the shape of the $\Delta R/R$ and $\Delta T/T$ spectra bear the unmistakable signature of FKO's associated with a 3D absorption edge. This is appreciated when comparing Fig. 13(a) with Fig. 3. Second, if we tried to fit the spectra with third or first derivative lineshapes we would need 6 transitions [horizontal lines in Fig. 13(c)] which cannot be explained by intersubband transitions for any value of the band offset parameter, as shown in Fig. 13(c). Finally, when plotting the energy positions of the alternating maxima and minima according to eq. (6), we obtain a straight line [inset of Fig. 13(a)] which yields **F** E 7 kV/cm (slope) and $E_0 = 1.414$ eV (intercept) for the absorption edge. This value of E_0 corresponds to the calculated absorption edge for $Q = 0.57$ [see Fig. 13(c)], in accordance with the results for many other samples of this type discussed in section IV.1.1. Hence, the results of Fig. 13 can all be consistently explained by the existence of a built-in dc-field of **F** E 7 kV/cm. The existence of this field regime is not by any means obvious. In the case under consideration (d $= 100\AA$, A = 37 meV) eq. (12) is satisfied since the built-in dc-field mentioned above yields f E 0.2. On the other hand, the heavy-hole miniband has a negligible dispersion ($\Delta_h \simeq 1.5$ meV) which means that this hole is completely localized by the field (f_h E 5). The electron-hole interaction, if strong enough, could now localize the electron as well if the external field is weak enough, i.e., if

$$eFa_0 \ll |E_{exc}| \tag{2}$$

when a_0 is the exciton radius. Hence, the field must satisfy two simultaneous requirements:

$$eFa_0 \geq |E_{exc}| \quad \text{and} \quad eFd \ll \text{A}. \tag{3}$$

In the case under discussion (with $a_0 \simeq 150$ Å and $|E_{exc}|$ E 4 meV) condition (14) is satisfied, but in a general case the appearance of FKO's depends on a delicate balance between field strength, exciton radius, superlattice period, exciton binding energy and miniband spread **(A)**. The observation of this effect is also made difficult in most superlattices, such as AlGaAs/GaAs, because the signal from the superlattice may be masked by oscillatory behavior originating in the bulk portions of the sample (substrate, buffer and capping layers)[81]. Transmission measurements performed in InGaAs/GaAs superlattice contain information ONLY from the superlattice region since the sample becomes opaque when the absorption edge of GaAs (which constitutes the bulk parts of the sarnple) is reached.

Once the existence of the Franz-Keldysh regime for this superlattice is established, the evolution of the spectra as a function of the electric field can be studied by sandwiching it between n^+ and p^+ GaAs layers and varying the electric field by applying a bias voltage (V_b) to this sandwich. Such experiment is reported in ref.[13] and representative modulated transmission spectra for different values of V_b are displayed in Fig. 14. Four bias-voltage regions (I to IV in order of decreasing V_b, i.e., increasing dc-electric field) are easily identifiable in these spectra. In region I [curve (a) in Fig. 14] the field is very weak and the spectra correspond to that of excitonic lineshapes (FDLS of a Gaussian absorption profile). The two structures which appear in the spectra (labelled A and B) of this field region correspond to minizone-center transitions between heavy-(HH) and light-(LH) hole states to the only conduction rniniband. These transition energies remain unaltered throughout this field region (see Fig. 15) and they coincide with those calculated by the envelope-function method with Q = 0.57. In region II we are in the intermediate or Franz-Keldysh regime [curve (b) in Fig. 14]. By plotting the positions of alternating maxima and rninima according eq. (6) [see inset in Fig. 16], we obtain both

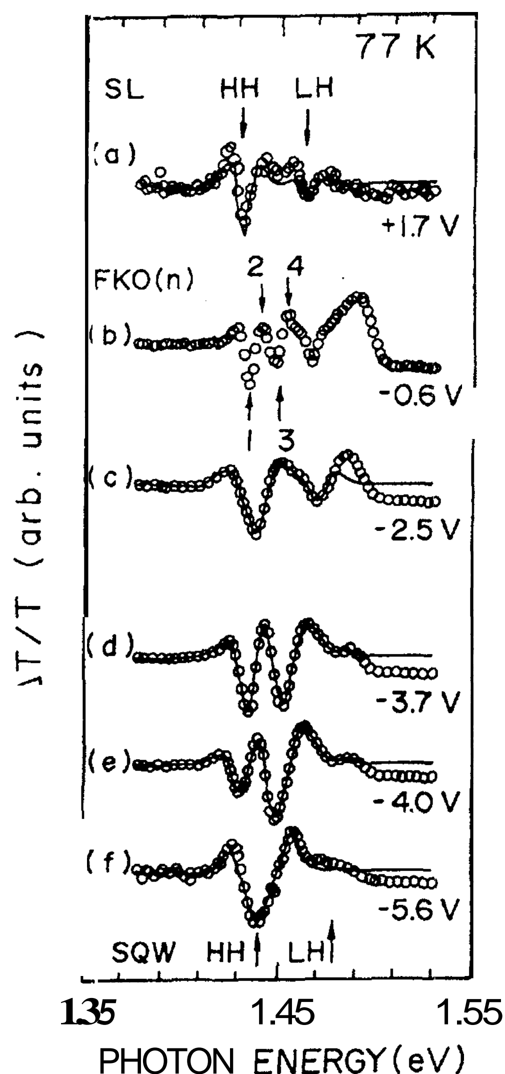

Figure 14: Modulated transmission (77 K) for different values of the applied bias voltage (V_b). Open circles represent experimental data while solid lines are TDLS fittings. Calculated heavy-(HH) and light-(LH) holes transitions for the superlattice (SL) or single quantum well (SQW) are indicated by arrows. FKO's are indexed (n = 1, 2, 3, ...) in (b).

the electric field and the absorption edge (E_0^{SL}) of the superlattice. The value obtained for E_0^{SL} is essentially independent of V_b (see Fig. 15) and coincides with that calculated for Q = 0.57. In region III [curve (c) in Fig. 14], only one Eroad line is observed in the neighborhood of the HH transition. The transition energy obtained by fitting this line increases markedly as F increases (V_b decreases), as shown in Fig. 15. Finally, in region IV, line A splits into three components whose transition energies obey the Stark-Wannier ladder relationship[13] :

$$E_n = E_0^{SQW} + neFd \quad (n = 0, \pm 1, ...), \qquad (1)$$

where E_0^{SQW} is the absorption edge of a field-free single quantum well of InGaAs. A representative plot of eq. (15) in region IV is shown in inset (a) of Fig. 16. The value of E_0^{SQW} obtained by this method is independent of V_b and coincides with the result of an envelope function calculation. The values of the electric field obtained from eq. (15) in region IV and eq. (6) in region II are shown in Fig. 16 as a function of bias voltage. The fact that field values in both regimes fall on the same straight line constitutes a self-consistency check on this interpretation. Thus, for the sample described in this experiment, the four field regions can now be expressed in terrns of the corresponding effective electric field ranges as:

(a) $0 \leq f \leq 0.08$ defines a regime in which spectral lines originate in transitions between mini-bands, modified by excitonic interaction;

(b) $0.08 \leq f \leq 0.21$ defines the Franz-Keldysh regime of intermediate fields where the effective-mass approximation can still be used;

(c) $0.21 \leq f \leq 0.29$ is a range in which the effective-mass approximation is no longer valid, but the wavefunction is not yet so localized as to be well described in the Stark-Wannier picture;

(d) $f \geq 0.3$, where the Stark-Wannier description is adequate and progress is shown from the formation of SWL's up to the total confinement of the wavefunction in a single QW [Fig. 14(f), $f \simeq 0.5$].

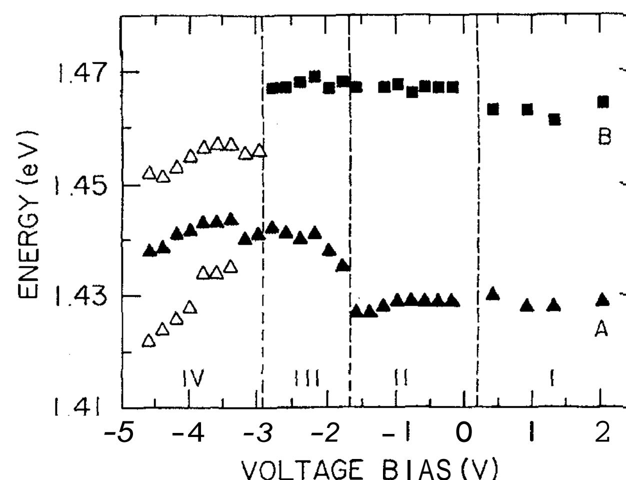

Figure 15: Transition energies obtained from fittingg lines A and B in the photomodulated transmission spectra at different values of the bias voltage.

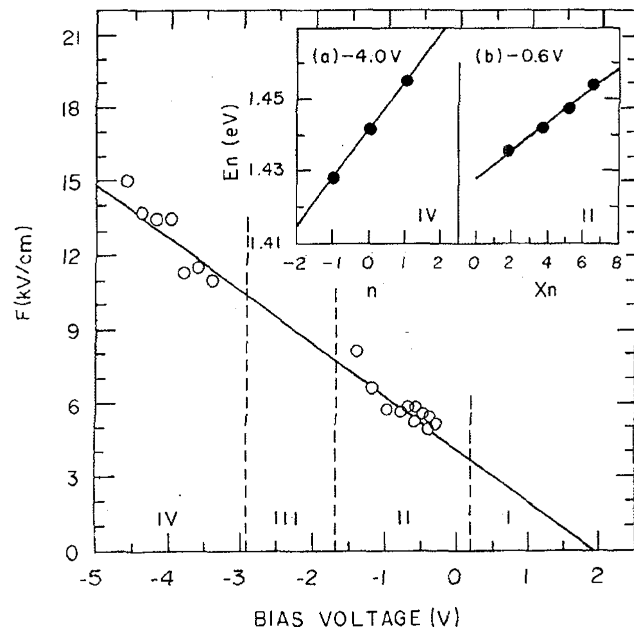

Figure 16: Electric fields obtained from eqs. (6) (region II) and (15) (region IV) in the text (open circles). The straight line is a linear regression fit to these points. Inset shows application of eqs. (6) and (15) to the calculation of F.

While the above results may not be universally valid, this step-by-step evolution of the electronic states as a function of the field constitutes a powerful starting point to a more complete understanding of the subject than was previously available.

IV.2.2. Two-Dimensional Electron Gas

The intense electric field which confines a two-dimensional electron gas (2DEG) in some semiconductor microstructures such as a modulation doped heterojunction (MDHJ) or GaAs samples with Si δ-doping may lead to a situation such as shown in Fig. 12(b), where the electrons are confined in quantized subbands while the holes are freely accelerated by the field. When the potential is narrow and only a small number of subbands exists, a quantum mechanical version of the Franz-Keldysh effect might take place. The modulated absorption or reflectivity spectra for these cases would contain only a finite number of oscillations whose periodicity would be governed by the field value at or around the Fermi energy of the 2DEG. From the number and periodicity of these oscillations, the intersubband spacings could be obtained. On the other hand, if the confining region is very wide, the surnmation over a large number of closely spaced quantized levels would reproduce the bulk situation of Fig. 12(a). These two cases define, for homogeneous fields, the bulk and quantum-confined versions of Franz-Keldysh effects. If, however, the field is very inhomogeneous, summing even over a small number of subbands would wash out the distinctive structures of the quantum-confined Franz- Keldysh effect (QCFKE). Thus, the observation of this effect depends critically on parameters such as the width of the space-cliarge region, homogeneity of the field, effective masses, etc. Based on a favorable coiijunction of these parameters, Zass et al.[84] have identified the structure observed in the 2-I< electroreflectance spectrum of a HgCdTe-MOS structure as a manifestation of QCFKE. Also, the photo and electroreflectance (T > 150 K) of some Al, $Ga_{1-x}As/GaAs$ MDHJ's have shown oscillations above the GaAs E_0 gap that were attributed to this effect[85–87]. Recently, Bernussi et al.[11] reported a series of photoreflectance measurements in $Al_xGa_{1-x}As/GaAs$ MDHJ and in a GaAs sample with Si 6-doping, performed over a wide temperature range ($14K \leq T \leq 300K$). Fig. 17 sliows typical photoreflectance spectra, where FKO's are plainly visible. By plotting the position of the alternating maxima and minima according to eq. (6) [inset of Fig. 17(a)] the temperature dependence of the field can be obtained as a function of temperature. This is shown in Fig. 17(b), where open triangles and squares are the fields obtained from the spectra for two different intensities of the modulating beam and the circles joined by a solid line represent a self-consistent calculation of the confining field at the Fermi energy[11]. The values of the field obtained from the spectra show a much sharper decrease, with decreasing temperature, than the theoretical field. This is particularly evident below 150 K, where the theoretical field starts saturating and reaches its lowest value (F E 22 kV/cm) at T E 20 K, while the experimental fields decreases linearly extrapolating to zero at T = 0 K. This discrepancy led the authors of ref.[11] to suggest that the observed oscillations are a bulk effect related to the fields at the surface of the GaAs capping layer or the interface between the GaAs substrate and the MBE deposited GaAs layer. Such fields have produced FKO's in photoreflection spectra of MBE GaAs layers and heterojunctions even in the absence of a 2DEG[88,89], some of which show a temperature dependente very similar to those as ref. [11]. These results cast some doubts on the validity of associating oscillations in the high temperature modulated reflectivity spectra of this type of sample with the quantum confined variety of Franz-Keldysh effect. Subsequently, photoreflectance measurements performed on a modulation-doped $Al_{0.35}Ga_{0.65}As/GaAs$ heterojunction containing a high mobility 2DEG confirmed these suspicions[12]. The measurements were carried at several temperatures ($2K \leq T \leq 300K$) and in a photon energy range covering the absorption edge of both the GaAs and the $Al_{0.35}Ga_{0.65}As$. FKO's were observed around both absorption edges, as shown in Fig. 18. From these FKO's the field on both sides of the heterojunction was determined for each value of the tem-

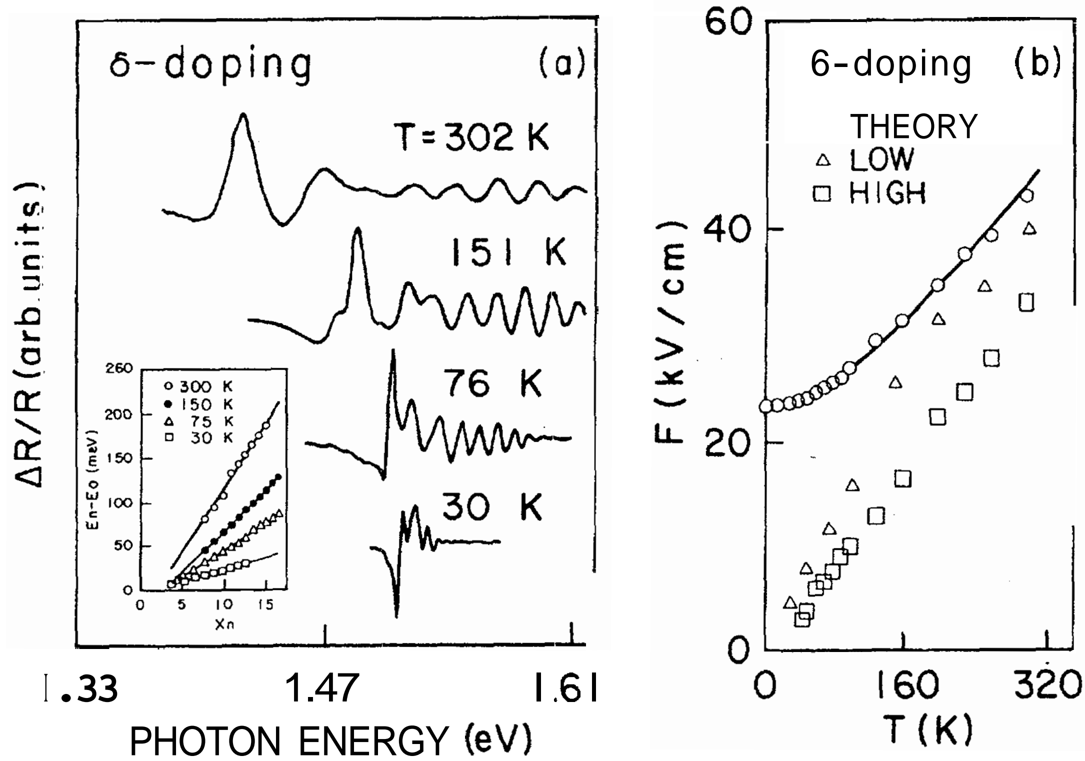

Figure 17: (a) Photoreflectance spectra of a GaAs sample with Si δ-doping; the inset shows plot of eq. (6) in the text from which electric field values are obtained. (b) Temperature dependence of the electric field obtained from PR spectra (squares and triangles) and theoretical calculations (circles and continuous line) of the confining field calculated at the Fermi energy.

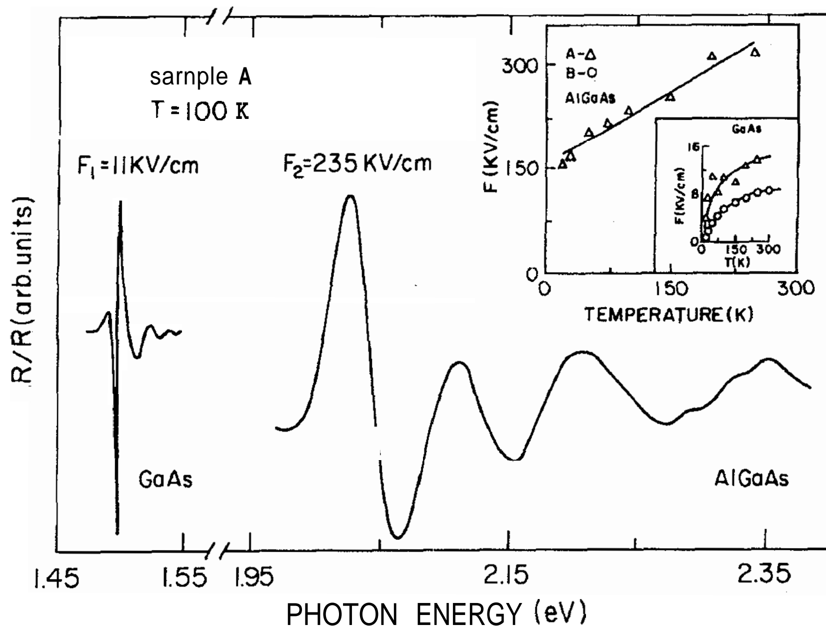

Figure 18: Photoreflectance spectrum of an $Al_{0.35}Ga_{0.65}As/GaAs$ MDHJ. The inset shows the temperature dependence of the electric fields F_1 and F_2 obtained from the FKO's on the GaAs and AlGaAs sides of the spectra. Also shown (circles) is the temperature dependence of the field present in an epitaxial GaAs sample with no heterojunction or 2DEG.

perature. The temperature dependence of the field on the AlGaAs side (F_2) is shown in the inset of Fig. 18 (triangles) while the field (F_1) obtained from the GaAs side of the spectra is shown in the lower right hand corner box (also as triangles). The AlGaAs layer of the sample used by Novellino et al.[12] was very thin, so the F_2 really represents the field on the alloy side of the heterojunction. If F_1, responsible for the observed FKO's of the GaAs absorption edge, were the same field as F_2 on the other side of the junction, then F_1 and F_2 would have comparable values and identical temperature dependence. This is clearly not so, as shown in the inset of Fig. 18. While F_2 decreases linearly as T decreases extrapolating to $F_2 \simeq 150$ kV/cm at T = 0 K, F_1 has a rapid decrease which extrapolates to zero at T = 0 K. In fact, this temperature dependence is analogous to that obtained by studying the FKO's of a GaAs sample (MOCVD-deposited GaAs on a semi-insulating GaAs substrate) with no 2DEG, shown as circles in the box of the inset in Fig. 18. This shows conclusively that the observed FKO's associated with the GaAs absorption edge do not originate in the region of the 2DEG. They are, rather, a bulk effect related to either the capping layer or the buffer-substrate interface. In the light of this discussion, it is doubtful that the quantum-confined Franz-Keldysh effect has in fact been observed up to the present time in this type of heterojunction.

V. Concluding Remarks

We have presented a review of recent work performed in our laboratories, in which the techniques of photo and electromodulated absorption and reflection were applied to a variety of problems in semiconductor microstructures. Although this is partial view of a much wider field, our discussion illustrates the strong and weak points of these techniques. High resolution spectra can be obtained with modest means even at room temperature. On the other hand, the interpretation of the spectra is non-trivial and calls for a good understanding of the physical situation under study. Straightforward generalizations of recipies that apply to bulk serniconductors can produce rnisleading results when studying the spectra of some microstructures. However, with due care, rich information can be obtained from these spectra.

References

1. M. Cardona, Modulation Spectroscopy, Solid State Physics Suppl. 11, ed. by F. Seitz and W. Turnbull (Academic Press, New York,1969). This book gives a comprehensive review of the early history, and experimental techniques and results.
2. Volume 9 of the series Semiconductors and Semimetals, ed. by K. Williardson and A. C. Beer (Academic Press, New York, 1972) contains several articles on the subject.
3. B. O. Seraphin, *Optical* Properties of Solids, ed. by F. Abeles (North Holland, Amsterdam, 1972).
4. D. E. Aspnes, Surf. Sci. **B10**, 4228 (1973).
5. D. E. Aspnes in Handbook on *Semiconductors,* ed. by T. S. Moss (North Holland, Amsterdam, 1980) p. 109.
6. F. H. Pollak, Superlattices and Microstructures 6, 203 (1989).
7. F. H. Pollak, Superlattices and Microstructures 10, 333 (1991).
8. C. Vázquez-López, E. Ribeiro, F. Cerdeira, P. Motisuke, M. A. Sacilotti and A. P. Roth, J. Appl. Phys. 69, 7836 (1991).
9. E. Ribeiro, C. Vázquez-López, F. Cerdeira, P. Motisuke, M. A. Sacilotti and A. P. Roth, Proceedings of the Fifth Brazilian School on Semiconductor Physics, ed. by J. R. Leite (World Scientific, Singapore, in print).
10. F. Cerdeira, C. Vázquez-López, E. Ribeiro, P. A. M. Rodrigues, V. Lemos, M. A. Sacilotti and A. P. Roth, Phys. Rev. B42, 9480 (1990).
11. A. A. Bernussi, C. A. C. Mendonça, P. Motisuke, E. A. Meneses, F. Cerdeira, F. H. Pollak, P. Basmaji and I. F. L. Dias, Proceedings of the 20th International Conference on the Physics of Semiconductors, ed. by E. M. Anastassakis and J. D. Joannopoulos (World Scientific, Singapore, 1990) p. 1065.
12. R. A. Novellino, C. Vázquez-López, A. A. Bernussi, C. Schrnidt, F. Cerdeira, P. Motisuke, F. H. Pollak, F. Meseguer and K. Ploog, J. Appl. Phys. 70, 5577 (1991).
13. E. Ribeiro, F. Cerdeira and A. P. Roth, Phys. Rev. B, 46, 12542 (1992).
14. P. A. M. Rodrigues, F. Cerdeira and J. C. Bean, Phys. Rev. B, 46, 15263 (1992).
15. F. Cerdeira and M. Cardona, Solid State Commun. 7, 879 (1969).
16. D. E. Aspnes, Solid State Commun. 8, 267 (1970).
17. D. E. Aspnes and A. A. Studna, Phys. Rev. **B7,** 4605 (1973).
18. C. van Hoof, K. Deneffe, J. De Boeck, D. J. Arendt and J. Borghs, Appl. Phys. Lett. 54, 608 (1989).
19. D. E. Aspnes and J. E. Rowe, Solid State Commun. **8,** 1145 (1970).
20. D. E. Aspnes and J. E. Rowe, Phys. Rev. B5, 4022 (1972).
21. D. E. Aspnes, Phys. Rev. Lett. 28, 168 (1972).
22. J. D. Dow in *Optical* Properties of *Solids:* New developments, ed. by B. O. Seraphin (North Holland, Amsterdam 1976) p. 33.
23. F. C. Weinstein, J. D. Dow and B. Y. Lao, Phys. Rev. B4, 1037 (1970).

24. D. E. Aspnes and A. Frova, Phys. Rev. E2, 1037 (1970).
25. See for example F. H. Pollak and M. Cardona, Phys. Rev. 172, 816 (1968).
26. M. H. Meynadier, R. E. Nahory and M. C. Tamargo, Solid State Commun. 63, 463 (1987).
27. H. Shen, P. Parayanthal, F. H. Pollak, M. Tomkiewicz, T. J. Drummond and J. N. Schulman, Appl. Phys. Lett. 48, 653 (1986).
28. P. Parayanthal, H. Shen, F. H. Pollak, O. J. Glembocki, E. V. Shanabrook and W. T. Beard, Appl. Phys. Lett. 48, 1261 (1986).
29. A. Kangarlu, H. R. Chandrasekhar, M. Chandrasekhar, F. A. Chambers, B. A. Vojak and J. M. Meese, Superlattices and Microstructures 2, 569 (1966).
30. R. C. Miller, D. A. Kleinman, W. A. Norland and A. C. Gossard, Phys. Rev. B22, 863 (1980).
31. D. A. B Miller, D. S. Chemla, D. J. Eilemberger, P. W. Smith, A. C. Gossard and W. T. Tsang, Appl. Phys. Lett. 41, 679 (1982).
32. D. S. Chemla, T. C. Damen, B. A. B. Miller, A. C. Gossard and W. Wiegmann, Appl. Phys. Lett. **42,** 864 (1983).
33. P. Dawson, G. Duggan, H. I. Ralph and K. Woodbridge, Phys. Rev. B28, 7381 (1983).
34. D. A. B Miller, D. S. Chemla, T. C. Damen, A. C. Gossard, W. Wiegmann, T. H. Woud and C. A. Burrus, Phys. Rev. **B32**, 1043 (1985).
35. B. V. Shanabrook, O. J. Glembocki and T. Beard, Phys. Rev. B5, 2540 (1987).
36. O. J. Glembocki and B. V. Shanabrook, Superlattices anc Microstructures 3, 235 (1987); ibid. 5, 603 (1983).
37. See comment at the bottom of p. 426 in ref.[4].
38. G. Bastard, Wave *Mechanics Applied* to Semiconductor Heterostructures (Les Éditions de Physique, France, 1989).
39. G.E.Marques, A.M.Cohen, P.A.M.Rodrigues, F.Iikawa P.Motisuke and F.Cerdeira, Proceedings of the 19th International Conference on the Physics of Semiconductors, in print.
40. Some of this work is reviewed in section 4(c) of ref.[7].
41. F. Iikawa, F. Cerdeira, C. Vázquez-López, P. Motisuke, M. A. Sacilotti, A. P. Roth and R. A. Masut, Phys. Rev. B38, 8473 (1988).
42. J. Menendez, A. Pinczuk, D. J. Werder, S. K. Sputz, R C. Miller, D. L. Svico and Y. Cho, Phys. Rev. **B36**, 8165 (1987).
43. J. Y. Marzin, M. H. Charasse and B. Sermage, Phys. Rev. **B31,** 8298 (1985).
44. G. Ji, D. Huang, U. K. Reddy, T. S. Henderson, R. Houdre and H. Morkoc, J. Appl. Phys. 62, 3366 (1987).
45. S. H. Pan, H. Shen, Z. Hang, F. H. Pollak, W. Zhuang, Q. Xu, A. P. Roth, R. A. Masut, C. Lacelle and D. Morris, Phys. Rev. B38, 3375 (1988).
46. G. Ji, W. Dobbelaere, D. Huang and H. Morkoç, Phys. Rev. B39, 3216 (1989).
47. U. K. Reddy, G. Ji, T. Henderson, D. Huang, R. Houdre and H. Morkoc, J. Vac. Sci. Technol. **B7**, 1106 (1989).
48. D. J. Arent, D. Deneffe, C. van Hoof, J. Deboeck and E. Borgms, J. Appl. Phys 66, 1739 (1989).
49. S. C. Shen, X. M. Fang and W. Fang, in Proceedings of The 20th International Conference on the Physics of Semiconductors, ed. by E. M. Anastassakis and J. D. Joanopoulos (World Scientific, Singapore, 1990), p. 921.
50. M. J. Joyce, M. J. Johnson, M. Gal and B. F. Usher, Phys. Rev. **B38,** 10978 (1988).
51. A. Ksendzov, H. Shen, F. H. Pollak and D. P. Bour, Surf. Sci. 228, 326 (1990); Solid State Cornmun. 73, 11 (1990).
52. H. Chu and C. Yang, Phys. Rev. B36, 2946 (1987).
53. H. Shen, S. H. Pan, F. H. Pollak, M. Dutta and T. R. AuCoin, Phys. Rev. B36, 9384 (1987).
54. R. Hull and J. C. Bean in Semiconductors and Semimetals, Vol 33, ed. by T. P. Pealsall (Academic Press, New York, 1991) p.1.
55. G. Abstreiter, K. Eberl, E. Friess, W. Wegscheider and R. Zachal, J. Crystal Growth 95, 431 (1989).
56. T. P. Pearsall, CRC Crit. Rev. Sol. St. Mat. Sci. 15, 551 (1989).
57. E. Kasper and F. Schaffler, in ref.[54], p. 223.
58. R. People and S. A. Jackson in Semiconductors and Semimetals, vol 32, ed. by T. P. Pearsall (Academic Press, New York, 1990) p. 119.
59. M. Cardona and N. E. Christensen, J. Vac. Sci. Technol. B6, 1285 (1988).
60. C. G. Van de Walle and R. M. Martin, Phys. Rev. B34, 5621 (1986).
61. L. Colombo, R. Resta and S. Baroni, Phys. Rev. B44, 5572 (1991).
62. R. People and J. C. Bean, Appl. Phys. Lett. 48, 538 (1986).
63. R. People, J. C. Bean, D. V. Lang, A. M. Sergent, H. L. Stormer, K. W. Wecht, R. T. Lynch and K. Baldwin, Appl. Phys. Lett. 45, 1231 (1984).
64. G. Abstreiter, H. Brugger and T. Wolf, Phys. Rev. Lett. 54, 2441 (1985).
65. G. P. Schwartz, M. S. Hybertsen, J. Bevk, R. G. Nuzzo, J. P. Mannaerts and G. J. Gualtieri, Phys. Rev. B39, 1235 (1989).
66. E. O. Kane in *Semiconductors* and *Semimetals*, ed. by K. Willardson and A. C. Beer (Academic Press, New York, 1966) Vol. 1, p. 75.
67. D. F. Nelson, R. C. Miller and D. A. Kleinman, Phys. Rev. B35, 7770 (1987); K. H. Yoo, L. R. Ram-Mohan and F. D. Nelson, ibid. *B39,* 12808 (1989).
68. R. People and S. K. Sputz, Phys. Rev. B41, 8431

(1990).
69. J. L. Pan, L. C. West, S. J. Walker, R. J. Malik and J. F. Walker, Appl. Phys. Lett. 57, 366 (1990).
70. C. L. Cesar, M. N. Islam, R. D. Feldman, R. F. Austin, D. S. Chemla, L. C. West and A. E. Di-Giovanni, Appl. Phys. Lett. 56, 283 (1990).
71. The subject has been reviewed by D. L. Smith and C. Mailhiot, Rev. Mod. Phys. 62, 173 (1990).
72. G. Bastard, Phys. Rev. B24, 5693 (1981).
73. F. Cerdeira, A. Pinczuk and J. C. Bean, Phys. Rev. B31, 1202 (1985).
74. T. P. Pearsall, F. H. Pollak, J. C. Bean and R. Hull, Phys. Rev. B33, 6821 (1986).
75. Y. Yin, D. Yan, F. H. Pollak, M. S. Hybertsen, J. M. Vandenberg and J. C. Bean, Phys. Rev. B44, 5955 (1991).
76. M. Garriga, M. Cardona, N. E. Christensen, P. Lautenschlager, T. Isu and K. Ploog, Phys. Rev. B36, 3254 (1987).
77. U. Schrnid, F. Lukeš, N. E. Christensen, M. Alouani, M. Cardona, E. Kasper, H. Kibbel and H. Presting, Phys. Rev. Lett. 65, 1933 (1990); U. Schmid, N. E. Christensen, M. Alouani and M. Cardona, Phys. Rev. B43, 14597 (1991); U. Schmid, J. Humliček, F. Lukeš, M. Cardona, H. Presting, H. Kibbel, E. Kasper, K. Eberl, W. Wegscheider and G. Abstreiter, Phys. Rev. B45, 6793 (1992).
78. The subject has been reviewed by E. E. Mendez and F. Agulló-Rueda, J. Lumin. 44, 223 (1989), where the relevant references are listed.
79. J. Bleuse, G. Bastard and P. Voisin, Phys. Rev. Lett 60, 220 (1988).
80. J. A. Brum and F. Agulló-Rueda, Surf. Sci. 229, 472 (1990).
81. P. Voisin, J. Bleuse, C. Bouche, S. Gaillard, C. Alibert and A. Regreny, Phys. Rev. Lett. 61, 1639 (1988).
82. E. E. Mendez, F. Agulló-Rueda and J. M. Hong, Phys. Rev. Lett. 60, 2426 (1988).
83. K. Satzke, G. Weiser and W. Stoltz, Phys. Rev. **B43,** 2263 (1991) and references therein.
84. M. Zass, R. Sismann and F. Koch, Proceedings of the 20th International Conference on the Physics of Semiconductors, ed. by E. M. Anastassakis and J. D. Joannopoulos (World Scientific, Singapore 1990), p. 1186.
85. O. J. Glembocki, B. V. Shanabrook, N. Bottka, W. T. Beard and J. Comas, Apply. Phys. Lett. 46, 970 (1985); SPIE Proc. 524, 86 (1984).
86. R. A. Hopfel, J. Shah, A. C. Gossard and W. Wiegmann, Appl. Phys. Lett. 47, 163 (1985).
87. J. M. V. Martins, L. M. R. Scolfaro, C. A. C. Mendonça, E. A. Meneses and J. R. Leite, Superlattices and Microstructures 10, 239 (1991).
88. N. Pan, X. L. Zheng, H. Hendriks and J. Carter, J. Appl. Phys 68, 2355 (1990).
89. C. R. Liu, J. R. Anderson, D. R. Stone, W. T. Bean and R. A. Wilson, Superlattices and Microstructures 8, 155 (1990).